Experimental performance of a piston expander in a small- scale organic Rankine cycle

2015 IOP Conf. Ser.: Mater. Sci. Eng. 90 012066

(http://iopscience.iop.org/1757-899X/90/1/012066)

Experimental performance of a piston expander in a small-scale organic Rankine cycle

JF Oudkerk, R Dickes, O Dumont and V Lemort

Thermodynamic Laboratory, University of Liège, Campus du Sart Tilman B49, B-4000 Liège

E-mail: jfoudkerk@ulg.ac.be

Abstract. Volumetric expanders are suitable for more and more applications in the field of micro- and small-scale power system as waster heat recovery or solar energy. This paper present an experimental study carried out on a swatch-plate piston expander. The expander was integrated into an ORC test-bench using R245fa. The performances are evaluated in term of isentropic efficiency and filling factor. The maximum efficiency and power reached are respectively 53% and 2 kW. Inside cylinder pressure measurements allow to compute mechanical efficiency and drown P-V diagram. A semi-empirical simulation model is then proposed, calibrated and used to analyse the different sources of losses.

1. Introduction

The piston expander is among the oldest displacement machines. It has been largely used during the Industrial Revolution and up to the beginning of the 20th century. There is currently a large regain of interest for piston expanders for small-scale steam and organic Rankine cycle systems, especially used in micro-CHP and waste heat recovery on internal combustion engines ([1], [2], [3], [4]). Piston expanders actually show some advantages over other expansion machines, such as larger built-in volume ratio, high achievable operating pressures and temperatures, their ability to ingest liquid and low rotational speeds. Among technologies of piston expanders, axial machines show the additional advantage to be compact, which makes them suitable for mobile applications. However, there is a lack of scientific and technical literature on such machines.

The present paper describes an experimental investigation conducted on a swash-plate piston expander, characterized by a total cylinder volume of 195 cm^3. The lubrication is ensured by an external oil loop with injection of oil at mains friction points. As represented in Figure 1, the admission and exhaust processes are achieved by means of systems that induce symmetrical ports opening and closing timings with respect to TDC (Top Dead Center) and BDC (Bottom Dead Center). This expander was tested over several operating conditions and the measured performance is analyzed and presented in this study. A semi-empirical model (lumped parameter model) of a piston expander is then proposed, calibrated and validated based on experimental data. This model is finally used to simulate the performance and to analyze the different sources of losses.

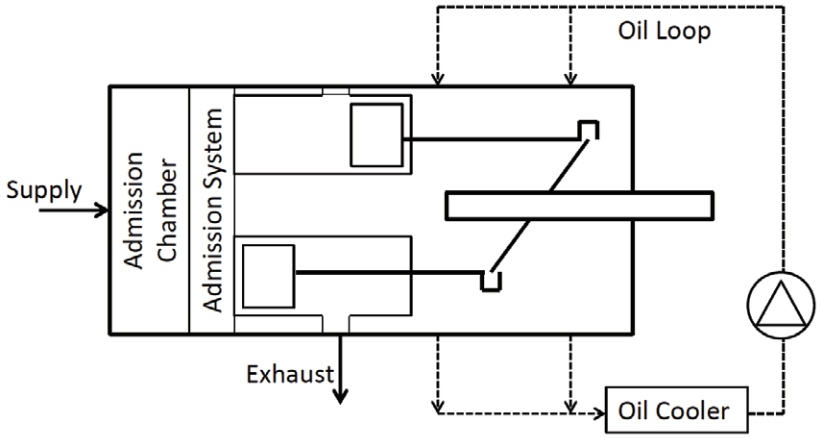

Figure 1: Schematic diagram of the swash-plate piston expander

2. Description of the test bench

The piston expander is integrated into an ORC cycle test bench using R245fa. Figure 2 represents this ORC composed of a pump, a recuperator, a boiler, a condenser and a liquid tank. The mass flow rate is controlled by adjusting the pump speed through a variable-frequency drive (VFD). The boiler is fed with thermal oil and the condenser is water-cooled.

The expander is connected to an asynchronous electrical motor. In order to start the expander and control its speed, the motor is driven by a four quadrants variable-frequency drive. As shown in Figure 2, several sensors are placed in order to measure the performance of the expander. The flow is measured at the pump outlet by a coriolis-effect mass flow meter. A torque sensor is placed between the expander and the generator in order to compute the mechanical power. Finally, the temperature and the pressure of the working fluid at the inlet and the outlet of the expander are measured with piezoresistive pressure sensors and Type-T thermocouples.

In addition of these measurements, the pressure in the cylinder is measured with the help of piezoelectric pressure sensor and the angular position of the shaft with a rotary encoder. This measurement system allows drawing P-V diagram and therefore indicated power and mechanical efficiency can be evaluated.

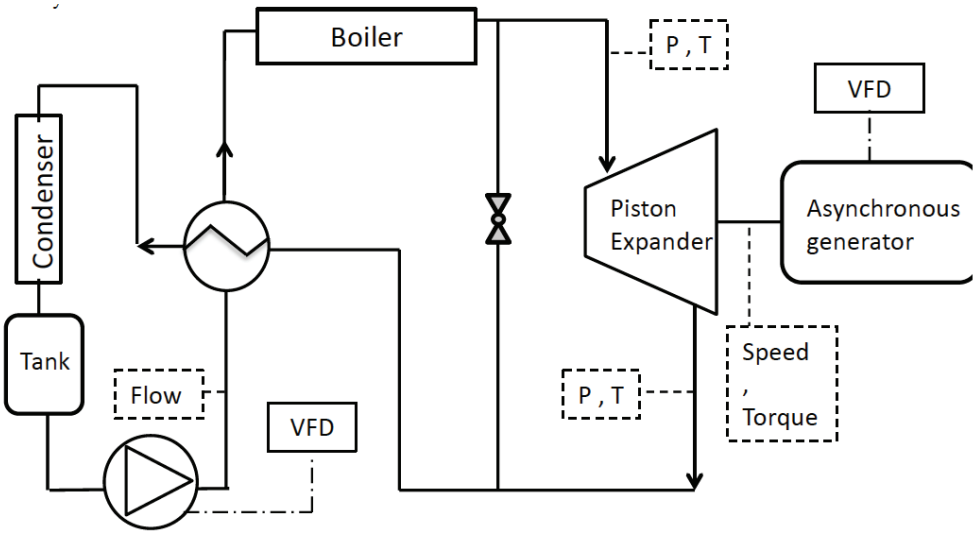

Figure 2: Schematic diagram of the test bench.

3. Experimental results

The initial goal of the experimentation was to test the expander for an exhaust pressure of 3bar, supply pressure varying from 18 to 30 bar and rotational speed from 1000 to 4000 RPM. Unfortunately, for high flow rate operating point, the pressure was higher than 3 bar due to the actual limitations of the test rig. Generally, the exhaust pressure varies along the achieved steady-state points. Table 1 shows the matrix of tests and the exhaust pressure obtained. The empty cases are operating conditions for which the expander consumes power and are not considered further.

Table 1 : Matrix test and exhaust pressure.

		Psu [bar]				
	Pex [bar]	18	21	24	27	30
RPM	1000	2.96	2.91	2.9	3.02	2.96
	2000		3.09	2.9	3.29	3.58
	2500		3.06	3,01	3,5	3.94
	3000		3.08	3.15	3.48	3.87
	3500		3.08	3.21	3.55	4.02
	4000		2.876	3.28	3.66	3.98

During the experimental campaign, a total of 60 steady-state operating points was measured. For a given rotational speed, the supply pressure is controlled by modifying the mass flow rate, which is imposed by the pump. The superheating is controlled by the oil boiler. For these points, the superheating was kept between 4 and 17 K, the mass flow rate varies from 29 to 105 g/s and the mechanical power output is comprised between 0.3 and 2 kW.

Figure 3 shows the evolution of shaft and indicated isentropic efficiencies in terms of pressure ratio. These isentropic efficiencies are respectively defined as the ratio between the measured shaft and indicated power and the isentropic power:

$$\epsilon_{s,sh} = \frac{\dot{W}_{\mathrm{sh}}}{\dot{M}.(h_{\mathrm{su,exp}} - h_{ex,exp,s})} \quad , \quad \epsilon_{s,in} = \frac{\dot{W}_{\mathrm{in}}}{\dot{M}.(h_{su,exp} - h_{ex,exp,s})} \tag{1}$$

where $\dot{M}$ is the mass flow rate, $h_{su,exp}$ the supply enthalpy and $h_{ex,exp,s}$ the isentropic exhaust enthalpy,

The mechanical power is computed with the help of the torque (T_m) and the rotational speed (N):

$$\dot{W}_{sh} = N.2.\pi.T_m \tag{2}$$

The indicated power is computed by integrating the pressure inside the cylinder (P_{cyl}) with the volume of the cylinder (V_{cyl}) over one revolution to obtain the indicated work. This work is then multiplied by the rotational speed to compute the power:

$$\dot{W}_{in} = N.\oint P_{cyl}.dV_{cyl} \tag{3}$$

The ratio between the shaft and the indicated power is the mechanical efficiency of the expander:

$$\eta_m = \frac{\dot{W}_{sh}}{\dot{W}_{in}} = \frac{\epsilon_{s,sh}}{\epsilon_{s,in}} \tag{4}$$

For low pressure ratios, the shaft isentropic efficiency sharply decreases while the indicated isentropic efficiency remains quite constant. This means a decrease of the mechanical efficiency. Indeed, by reducing the pressure ratio, the indicated power decreases and the constant mechanical losses take more and more part leading to a decrease of the mechanical efficiency. The isentropic efficiencies also vary with the rotational speed. The indicated efficiency is lower for 1000 RPM. This can be explained by, as shown below, a larger impact of internal leakages for low rotational speeds. However, these leakage losses are balanced by a better mechanical efficiency and lower supply pressure drop for low rotational speed. This leads to the conclusion that a tradeoff can be made in order to find an optimal rotational speed.

Figure 3 also shows that, as expected because of the limitation of the test rig, high pressure ratio is achieved for 1000 RPM while it is limited for higher rotational speed. Further work should test the expander under higher pressure ratios at higher rotational speeds.

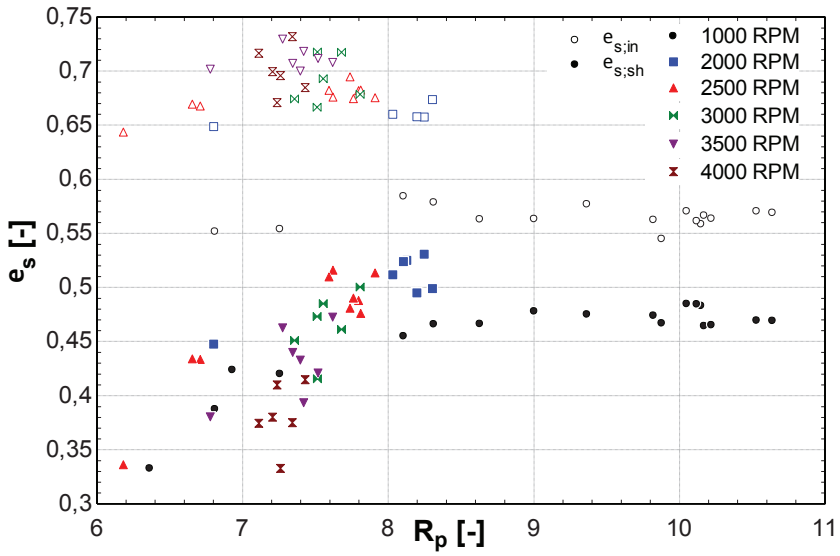

Figure 3 : Evolution of the shaft and indictaed isentropic efficiencies with the pressure ratio

The filling factor is used to evaluate the volumetric performance. The filling factor is defined as the ratio between the measured mass flow rate and a theoretical mass flow rate, computed based on the expander displacement:

$$FF = \frac{\dot{M}}{N.\rho_{su}.V_{IC}} \tag{5}$$

where N is the rotational speed, ρ_{su} the density at the inlet and V_{IC} the inlet closing volume defined as the cylinder volume when the intake port closes (see Figure 5).

As it can be seen in Figure 4, the filling factor increases with the pressure ratio and decreases with the rotational speed. The evolution with the speed is due to the increase of the leakage and the decrease of the supply pressure drop for low rotational speed. The value of the filling factor is always lower than 1 despite of the leakage. This is due to the presence of a clearance volume in the cylinder. So when the fluid is admitted in the cylinder, a part of the volume is already taken by some fluid trapped into this clearance volume. The effect of the clearance volume decreases when the pressure ratio increases because the mass flow increases and the then, the amount of fluid trapped into the clearance volume have less impact. Indeed, for a given exhaust pressure, the amount of fluid trapped into the clearance volume remain slightly constant while the mass flow increases with the supply pressure.

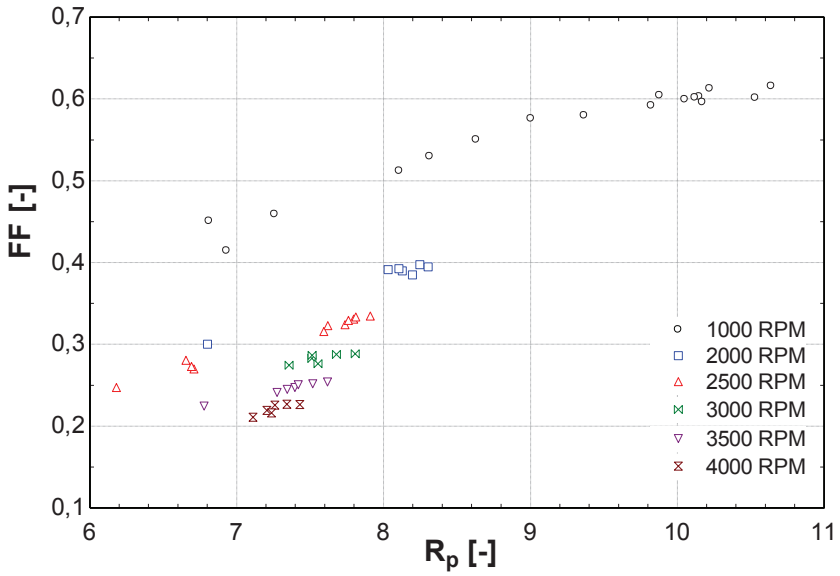

Figure 4 : Evolution of the filling factor with the pressure ratio

Figure 7 and Figure 8 show P-V diagram drawn with the measured in cylinder pressure for four operating conditions, two supply pressures and two rotational speeds. The inlet and exhaust closing volumes (V_{IC} and V_{EC}) shown on these figures are also the opening volumes (V_{IO} and V_{EO}) because of the symmetry of the admission and exhaust system. The evolution of the pressure drop with the speed and the supply pressure can be observed.

4. Piston expander semi-empirical model

The piston expander model, proposed by Glavatskaya et al. [1] and based on the semi empirical model of a scroll-expander proposed by Lemort et al. [5], has been adapted to represent the investigated swash-plate expander. The major difference between the modeling of a scroll and a piston expander lies in the presence of a clearance volume in the latter machine, which is responsible for the recompression of part of the fluid after the exhaust process. This difference yielded a modification of the scroll expander model to take into account the recompression process.

As in the scroll model, the evolution of the fluid through the expander is decomposed into six steps standing for the main physical features. The suction and the discharge processes are both considered as consecutive adiabatic pressure drop and isobaric cooling down (or heating up). After the suction process, the mass flow is split into two parts. The biggest part, the internal flow, following the expansion processes while the other one, the leakage flow, by-passes this expansion process. These two flows are mixed in an adiabatic way just before the discharge process.

Adiabatic pressure drops are computed assuming an isentropic flow through a convergent nozzle. The cross-sectional areas of the supply and exhaust fictitious nozzles are A_{su} and A_{ex}. Heat transfers are modeled as transfers between the fluid (or ambient air for ambient loses) and a fictitious wall, at uniform temperature, with overall heat transfer coefficients AU_{su}, AU_{ex} and AU_{amb}.

More information about the overall model can be found in [5]. The present paper focuses on the internal expansion process. The latter is divided in six steps as proposed by Stumpf [6] and shown in Figure 5:

- 1-2: isobaric intake
- 2-3: isentropic expansion
- 3-4: constant machine volume expansion
- 4-5: isobaric exhaust

- 5-6: isentropic compression
- 6-1: constant machine volume compression

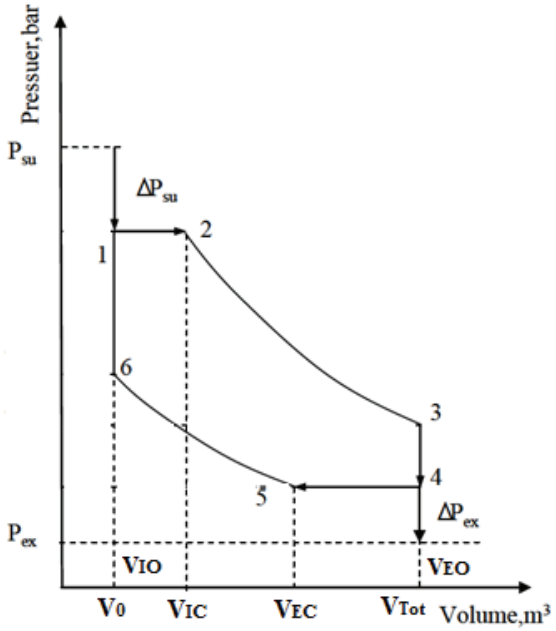

Figure 5 : Expansion process

This expansion process differs of the one of the studied expander. Indeed, as evoked above, the opening and closing volume are symmetric compared to TDC and BDC. In other words, during the compression stroke 5-6, the intake port opens at the same volume as in point 2 (see Figure 6) before the piston reaches the TDC. In the same way, during the expansion stroke 2-3, the exhaust port opens at volume in point 5 before the piston reaches the BDC.

The thermodynamic state of the fluid in point 2 is equal to that of the entering fluid (after pressure drop and heat transfer). The state at point 3 is computed with an isentropic expansion.

In the same way, the state of the fluid at point 5 is assumed to be the state just before the mixing with leakage flow. An isentropic compression allows computing the state at point 6.

The indicated work of the expansion cycle is given by the area under the PV diagram. This area can be computed by summing these four terms:

$$W_{in} = \frac{V_2}{v_2}.(h_2 - h_3) + V_{Tot}.(P_3 - P_4) - \frac{V_5}{v_5}.(h_6 - h_5) - V_0.(P_1 - P_6) \quad (6)$$

where $V_2 = V_{IC}$ is the intake closing volume, $V_5 = V_{EC}$ the exhaust closing volume, V_0 the clearance volume and v_2 and v_5 are specific volumes. V_{IC} and V_{EC} are defined with the following geometrical parameters:

$$f_{IC} = \frac{V_{IC}}{V_{Tot}} \;\; ; \;\; f_{EC} = \frac{V_{EC}}{V_{Tot}} \quad (7)$$

The enthalpy at point 5 is computed by the energy balance over the expansion process:

$$\dot{W}_{in} = \dot{M}_{in}.(h_2 - h_5) \quad (8)$$

The mass flow depends on geometric parameters and operating conditions:

$$\dot{M} = \dot{M}_{in} + \dot{M}_{leak} = N.\left(\frac{V_{IC}}{v_2} - \frac{V_{EC}}{v_5}\right) + \dot{M}_{leak} \quad (9)$$

where the leakage flow rate ($\dot{M}_{leak}$) is computed in a similar way than the pressure drops, i.e. by introducing a fictitious nozzle of throat cross sectional area A_{leak}. The internal flow rate ($\dot{M}_{in}$) is computed by subtracting the mass trapped in the clearance volume out of the mass in the cylinder at the beginning of the expansion.

This model allows computing the indicated power but for the shaft power a model of the mechanical losses is needed. As suggested by Navaro for reciprocating compressor [7], the mechanical loss power is a function of indicated power and rotational speed:

$$\dot{W}_{loss} = A.\dot{W}_{in} + B.RPM^2 \quad (10)$$

The coefficient A and B are determined with linear regression. A coefficient of determination of R^2=98.9 % was obtained with A =0.1427 [-] and $B = 4.5682.10^{-5}$ $[W.min^2]$.

Finally, the model requires five inputs: the supply and exhaust pressures, the supply and ambient temperatures and the rotational speed. The main outputs are the mass flow rate, the shaft power and the exhaust temperature. The six parameters of the model, given in Table 1, are tuned to obtain the best fit with the measurements.

Table 1: Calibrated parameters of the model

A_{su} $[mm^2]$	A_{ex} $[mm^2]$	A_{leak} $[mm^2]$	AU_{su} $[W/K]$	AU_{ex} $[W/K]$	AU_{amb} $[W/K]$
2.01	78.54	0.237	$1.\left(\frac{\dot{M}}{0.013}\right)$	$2.\left(\frac{\dot{M}}{0.013}\right)$	4

With these parameters, the error is below 5% for mass flow and shaft power and 5K for exhaust temperature. The comparison between measured and calculated outputs is shown on Figure 6.

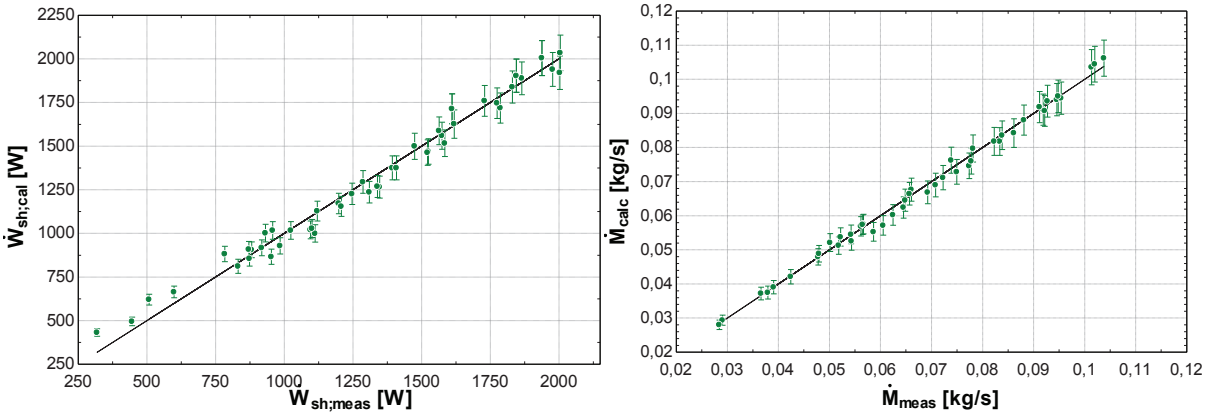

Figure 6 : Comparison between measured and calculated values of shaft power and mass flow rate

Figure 7 and Figure 8 show comparison of P-V diagrams predicted by the model and those measured. As it can be seen, the calculated diagrams are closed to the measured despite of the difference of the expansion process (different opening and closing volume).

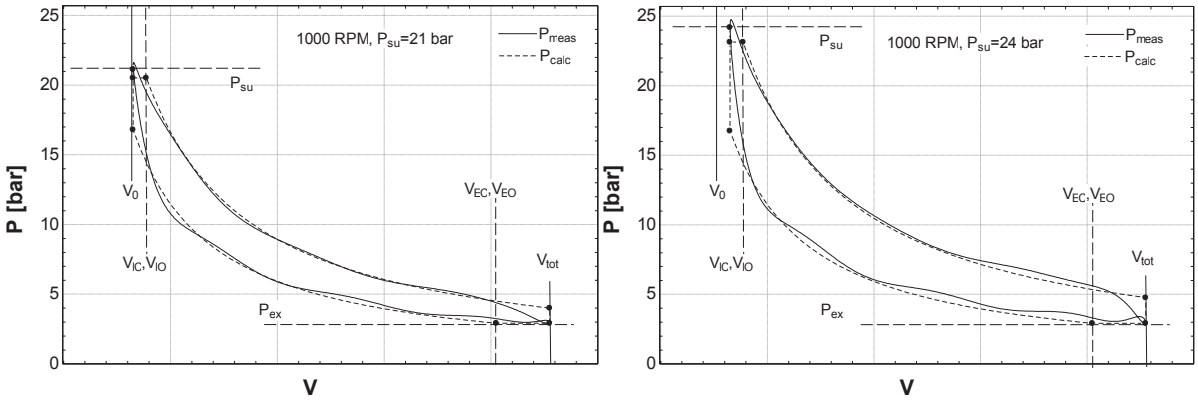

Figure 7 : P-V diagrams for RPM=1000 and for $\boldsymbol{P_{su} = 21}$ bar (left) and $\boldsymbol{P_{su} = 24}$ bar (right)

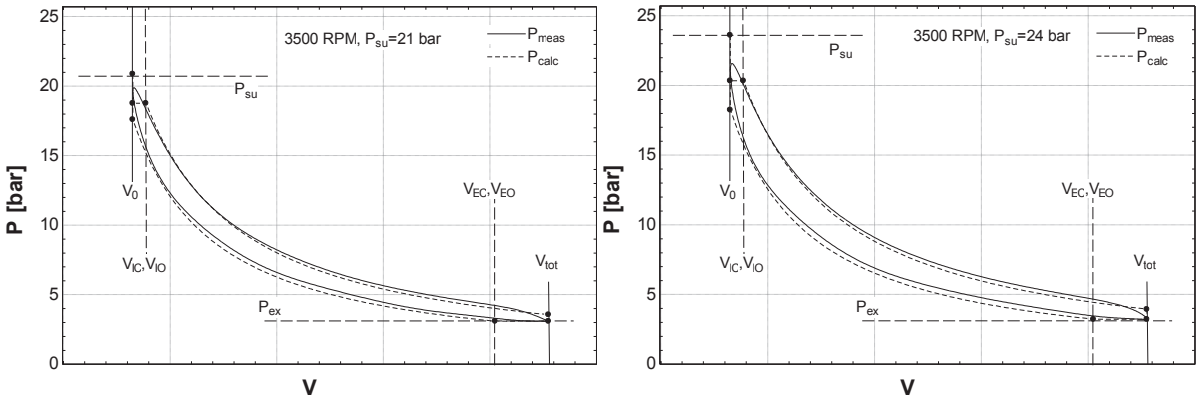

Figure 8 : P-V diagrams for RPM=3500 and for $\boldsymbol{P_{su} = 21}$ bar (left) and $\boldsymbol{P_{su} = 24}$ bar (right)

5. Model analysis

5.1. Decomposition of the losses

The model is used to analyse the impact of each source of losses on the isentropic efficiency. Figure 9 shows disaggregation of different losses. First, it can be seen that the built-in volume ratio leads to a decrease of the isentropic efficiency with the pressure ratio due to under expansion losses. For a pressure ratio of 5.8, the work to compress the fluid trapped into the clearance volume becomes equal to the work produced during the expansion and then the expander cannot produce anymore power. Then, different sources of losses are added. Heat transfers slightly decrease the performances. The leakages have a strong impact on the efficiency and flatten the curve because they have more impact at low pressure ratios. The pressure drop does not impact much more the efficiency because the power and the flow rate decrease in the same time. The pressure drop affects more the compactness of the expander. Finally, the mechanical losses decrease the efficiency and, as observed on the measurement, have more impact for low pressure ratios.

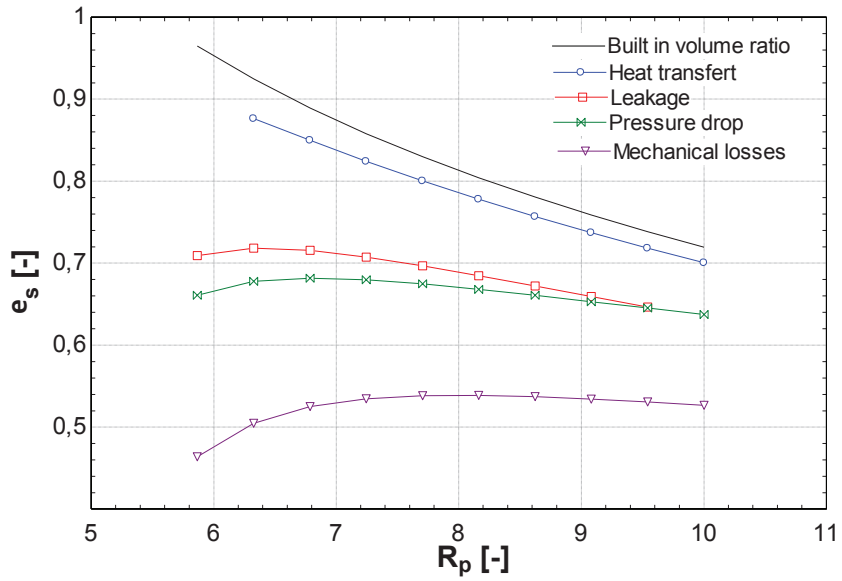

Figure 9 : Impact of each source of losses on the isentropic efficiency

5.2. Optimal rotational speed

Figure 10 shows the evolution of mechanical efficiency, leak ratio (which is the ratio between the leakage flow rate and the total mass flow rate) and isentropic efficiencies in terms of rotational speed. It can be seen that, when rotational speed increases, the leak ratio decreases leading to an increase of indicated isentropic efficiency. However, at the same time, the mechanical efficiency decreases. These two opposite effects lead to a rotational speed that maximises the isentropic efficiency. This optimal speed is 2000 RPM and doesn't change with the supply pressure. That corresponds to a mean piston speed of 2 m/s.

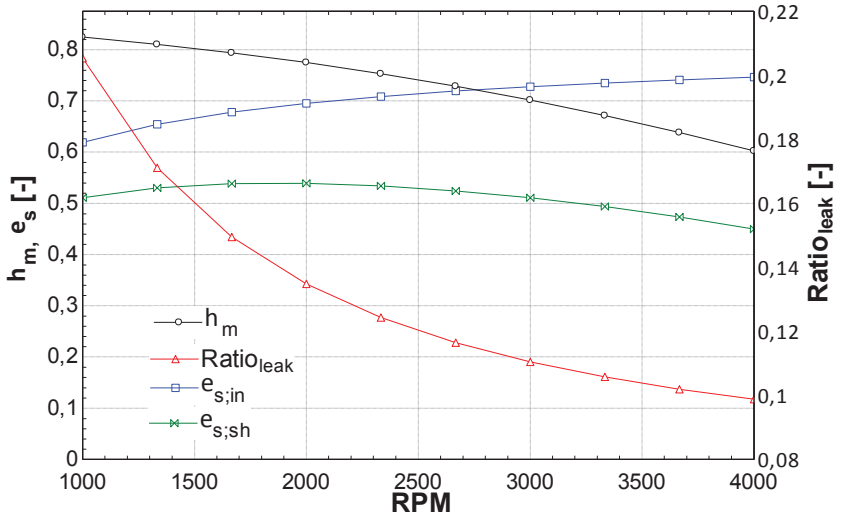

Figure 10 : Influence of rotational speed on isentropic efficeincy for $\mathbf{P_{su} = 24}$ bar and $\mathbf{P_{ex} = 3}$ bar

6. Conclusion

A swash-plate piston expander was tested in an ORC system with R245fa. Measurement of inside cylinder pressure allowed computing indicated power and thus mechanical efficiency. The maximal achieved isentropic efficiency was 53 %. The filling factor was always below 1 despite of leakage because of the clearance volume. The mechanical efficiency is comprised between 50 and 85% and is

strongly related to the shaft torque. Unfortunately the test rig did not allow reaching high pressure ratio for high RPM.

A semi-empirical model of a scroll expander was adapted to describe the piston expander. The model is able to predict measured mass flow rate and mechanical power within 5%. This model was used to analyse the different source of losses and determine the optimal rotational speed.

References

[1] Glavatskaya Y, Podevin P, Lemort V, Shonda O, Descombes G 2012 Reciprocating Expander for an Exhaust Heat Recovery Rankine Cycle for a Passenger Car Applicatio *Energies* **5**(6) 1751-1765

[2] Seher D, Lengenfelder T, Gerhardt J, Eisenmenger N, Hackner M, Krinn I 2012 Waste Heat Recovery for Commercial Vehicles with a Rankine Process, 21st Aachen Colloquium Automobile and Engine Technology

[3] Daccord R, Melis J, Kientz T, Darmedru A, Pireyre R, Brisseau N, Fonteneau E 2013 Exhaust heat recovery with rankine piston expander In Proceedings of ICE Powertrain Electrification & Energy Recovery, Rueil-Malmaison, France, 28 May 2013

[4] Wronski J, Skovrup M J, Elmegaard B, Risla H N, Haglind F 2012 Design and Modelling of a Novel Compact Power Cycle for Low Temperature Heat Sources, In Proceedings of ECOS 2012, The 25th International Conference on Efficiency, Cost Optimization, Simulation and Environmental Impact of Energy Systems, June 26-29, 2912, Perugia, Italy

[5] Lemort V, Quoilin S, Cuevas C, Lebrun J 2009 Testing and modeling a scroll expander integrated into an Organic Rankine Cycle *Applied Thermal Engineering* **29** 3094-3102

[6] Stumpf J. 1922 *The una-flow steam-engine*, Second Edition

[7] Navarro E, Granryd E, Urchueguia JF, Corberan JM 2007 A phenomenological model for analyzing reciprocating compresors *International Journal of Refrigeration* **30** 1254-1265